Calcium Binding by the N-Terminal Cellulose-Binding Domain from *Cellulomonas fimi* β-1,4-Glucanase CenC†

Philip E. Johnson,[‡,§] A. Louise Creagh,[‡,||,⊥] Emmanuel Brun,[‡,§] Koman Joe,[‡,§] Peter Tomme,[‡,||,#] Charles A. Haynes,[‡,||,⊥] and Lawrence P. McIntosh*[,‡,§]

Protein Engineering Network of Centres of Excellence, The Biotechnology Laboratory, Department of Chemical Engineering, Department of Biochemistry and Molecular Biology, Department of Chemistry, and Department of Microbiology and Immunology, The University of British Columbia, Vancouver, British Columbia, Canada V6T 1Z3

Received April 29, 1998; Revised Manuscript Received June 25, 1998

ABSTRACT: The interaction of the N-terminal cellulose-binding domain, CBD_{N1}, from *Cellulomonas fimi* β-1,4-glucanase CenC with calcium was investigated using NMR spectroscopy and calorimetry. CBD_{N1} binds a single calcium ion with an equilibrium association constant of approximately 10^5 M^{-1} at 35 °C and pH 6.0. Binding is exothermic (-42 ± 2 kJ mol^{-1}) under these conditions and is accompanied by a small negative change in heat capacity ($\Delta C_p = -0.41 \pm 0.16$ kJ mol^{-1} K^{-1}). From an NMR line shape analysis, the rate constants for calcium association and dissociation were found to be $(5 \pm 2) \times 10^7$ s^{-1} M^{-1} and $(4.5 \pm 0.6) \times 10^2$ s^{-1}, respectively. The rapid association kinetics indicate that the calcium-binding site on CBD_{N1} is accessible and, to the first approximation, preformed. Based on patterns of chemical shift perturbations, and structural comparisons with the *Bacillus sp.* 1,3-1,4-β-glucanases, the backbone carbonyl oxygens of Thr8, Gly30, and Asp142 and a side chain carboxyl oxygen of Asp142 are postulated to form the calcium-binding site of CBD_{N1}. Consistent with the calcium-independent affinity of CBD_{N1} for cellopentaose, this exposed site is located on the face of CBD_{N1} opposite to that forming the oligosaccharide-binding cleft. The midpoint denaturation temperature of CBD_{N1} is increased by approximately 8 °C at pH 6.0 in the presence of saturating amounts of calcium, confirming that metal ion binding is thermodynamically linked to native-state stability.

Enzymes that degrade cellulose often contain one or more domains that mediate binding to this complex substrate (*1*). Over 200 putative cellulose-binding domains (CBDs)[1] have been identified and classified into 13 families based on their sequence similarity (*2*). In particular, the N-terminal family IV CBD from *Cellulomonas fimi* β-1,4-glucanase CenC (CBD_{N1}) has been extensively studied. CBD_{N1} has a unique specificity in that it binds to amorphous cellulose, soluble cellooligosaccharides, and a variety of soluble glucans, but not to crystalline cellulose (*3*−*5*). The structure of CBD_{N1} is comprised of two five-stranded β-sheets that fold into a jellyroll β-sandwich (*6*). The oligosaccharide-binding site is formed by a cleft that runs across one β-sheet face of the protein. The presence of this cleft, into which single stands of sugar can lie, explains the selectivity of CBD_{N1} for amorphous cellulose. In contrast, CBDs that interact with crystalline cellulose have a flat binding surface with three solvent-exposed aromatic side chains (*7*−*9*).

During a previous NMR study of oligosaccharide-free CBD_{N1}, it was noted that resonances from 13 amides at its N-terminus and near its single disulfide bond (Cys33−Cys140) were not observed in a $^1H-^{15}N$ HSQC spectrum due to severe exchange broadening (*4*). Signals from these amides were detected only upon addition of excess cellotetraose, but not any other cellooligosaccharide. Subsequent investigations revealed that the cellotetraose was contaminated by a substance that bound to CBD_{N1} and caused the exchange-broadened amide resonances to appear. At the same time, we noted that CBD_{N1} shares a common fold with a number of other proteins including the 1,3-1,4-β-glucanases from *Bacillus sp.* (*10*−*12*), and the CBDs from *Clostridium thermocellum* scaffoldin subunit Cip A (CBD_{Cip}; *9*) and *Thermomonospora fusca* endo/exocellulase E4 (CBD_{E4}; *13*). Each of these proteins was found to contain a bound calcium ion. We therefore suspected that CBD_{N1} also binds calcium

† This work was supported by the Canadian Network of Centres of Excellence program with funding from the Medical Research Council of Canada and the Natural Sciences and Engineering Research Council of Canada.

* To whom correspondence should be addressed at the Department of Biochemistry and Molecular Biology, 2146 Health Sciences Mall, The University of British Columbia, Vancouver, British Columbia, Canada V6T 1Z3. Phone: (604) 822-3341. E-mail: mcintosh@otter.biochem.ubc.ca.

‡ Protein Engineering Network of Centres of Excellence.

§ Department of Biochemistry and Molecular Biology and Department of Chemistry.

|| The Biotechnology Laboratory.

⊥ Department of Chemical Engineering.

Department of Microbiology and Immunology.

[1] Abbreviations: CBD_{Cip}, cellulose-binding domain from *Clostridium thermocellum* scaffoldin subunit Cip B; CBD_{E4}, cellulose-binding domain from *Thermomonospora fusca* endo/exocellulase E4; CBD_{N1}, N-terminal cellulose-binding domain from *Cellulomonas fimi* β-1,4-glucanase CenC; CBD_{N1}·Ca^{2+}, 1:1 complex of CBD_{N1} and calcium; CBD_{N2}, cellulose-binding domain from *Cellulomonas fimi* β-1,4-glucanase CenC following CBD_{N1} in sequence; CBD_{N1N2}, tandem cellulose-binding domains from *Cellulomonas fimi* β-1,4-glucanase CenC; HSQC, heteronuclear single quantum correlation; pH*, observed pH meter reading without correction for isotope effects; T_m, midpoint temperature of the unfolding transition.

S0006-2960(98)00978-7 CCC: $15.00
Published on Web 08/22/1998

and that the sample of cellotetraose was contaminated with this metal ion.

Using NMR and calorimetry, we have confirmed that CBD_{N1}, both as an isolated domain and in tandem with the second CBD from CenC (CBD_{N1N2}), binds calcium and other divalent cations. The stability of CBD_{N1} is increased in the presence of calcium, while its affinity for cellopentaose remains unaffected. This paper reports a detailed structural, thermodynamic, and kinetic analysis of the interactions of CBD_{N1} and CBD_{N1N2} with this metal ion.

MATERIALS AND METHODS

Sample Preparation. Samples of unlabeled and 99% ^{15}N-labeled CBD_{N1} were prepared as described previously (*4*, *6*). Samples of CBD_{N2} and CBD_{N1N2} were prepared in a similar manner as CBD_{N1}, and will be described in detail elsewhere. To remove metal ions, all buffers were passed over a Chelex-100 column, and all plasticware, glassware, and NMR tubes were soaked overnight in 4 M HCl and then thoroughly rinsed with deionized water. Metal ions were removed from the protein samples by the addition of excess EDTA, followed by extensive buffer exchange using a Microsep concentrator or by size-exclusion HPLC with a Waters Protein-Pak 125 column. Protein concentrations were determined using measured ϵ_{280} values of 21 370 M^{-1} cm^{-1} (CBD_{N1}; *6*), 20 500 M^{-1} cm^{-1} (CBD_{N2}), and 40 740 M^{-1} cm^{-1} (CBD_{N1N2}).

NMR Spectroscopy. The buffer used for the NMR experiments presented in this study was 50 mM sodium chloride, 50 mM sodium [$^2H_3$]acetate, 0.02% sodium azide, 10% D_2O/90% H_2O at pH* 6.0. Acetate binds calcium weakly, with a K_a of ca. 100 M^{-1} (Brian Sykes, personal communication), and thus does not compete significantly with CBD_{N1}. Experiments were performed on a Varian Unity 500 MHz spectrometer equipped with a triple-resonance probe and pulsed field gradients. Enhanced-sensitivity pulsed field gradient $^1H-^{15}N$ HSQC experiments with selective water flip-back pulses (*15*) were recorded with uniformly ^{15}N-labeled proteins. All spectra were recorded at 35 °C and analyzed using a combination of NMRPipe, NMRDraw (*14*), and FELIX (Biosym Technologies).

Determination of Binding Constants by NMR Spectroscopy. The binding of calcium to CBD_{N1} and CBD_{N1N2} at 35 °C and pH* 6.0 was measured quantitatively using $^1H-^{15}N$ NMR spectroscopy. A 0.5 M stock solution of $CaCl_2$ was prepared by weight from the anhydrous salt in the same buffer as used for the protein samples. The pH* was maintained at 6.0. Ten $^1H-^{15}N$ HSQC spectra of CBD_{N1} (initially 1.4 mM) with increasing concentrations of calcium (final concentration 7.1 mM) were acquired as 512 × 96 complex points in the ^1H and ^{15}N dimensions with spectral widths of 7000 and 1650 Hz, respectively. Fourteen $^1H-^{15}N$ HSQC spectra of CBD_{N1N2} (initially 0.48 mM) with increasing concentrations of calcium (final concentration 1.5 mM) were acquired in a similar manner.

The association constant of fully calcium-loaded CBD_{N1} ($CBD_{N1}{\cdot}Ca^{2+}$) with cellopentaose was also measured using the methods outlined by Johnson et al. (*4*). Ten $^1H-^{15}N$ HSQC spectra of CBD_{N1} (initially 1.3 mM) in the presence of 7.1 mM calcium with increasing concentrations of cellopentaose (Seikagaku Corp.; final concentration 13 mM) were acquired using 512 × 96 complex points in the ^1H and ^{15}N dimensions with spectral widths of 6500 and 1450 Hz, respectively.

Equilibrium association constants were determined by nonlinear least-squares fitting of the chemical shift data versus the total added concentration of calcium or cellopentaose to the Langmuir isotherm describing the binding of one ligand molecule to a single protein site (*4*). The data were fit using the program PLOTDATA (TRIUMF, UBC, Vancouver).

Determination of Binding Constants by Isothermal Titration Calorimetry. Isothermal titration calorimetry (ITC) was performed using a Microcal MCS ITC. All samples were pH 6.0 in 50 mM sodium acetate and 50 mM sodium chloride, except in one case where sodium was replaced by tetramethylammonium ion as the buffer cation. Titrations were performed by injecting 26 consecutive 10 μL aliquots of a stock $CaCl_2$ solution into the ITC cell (volume = 1.3528 mL) containing calcium-free CBD_{N1}. Five independent titration experiments were performed at 35 °C to determine the binding constant for calcium by CBD_{N1}. Binding stoichiometry, enthalpy, and equilibrium association constants were determined by fitting the data, corrected for the heat of dilution of the titrant, to a 1:1 bimolecular interaction model. Three additional titrations were performed at 25, 30, and 40 °C to measure the heat capacity of binding.

Differential Scanning Calorimetry. Differential scanning calorimetry (DSC) was performed with a NanoDSC (Calorimetry Sciences Corp.) using a scanning rate of 1.0 K min^{-1}. Two CBD_{N1} samples in 50 mM cacodylate buffer, pH 6.0, were analyzed, either in the presence of a 100-fold molar excess of EDTA (apo-CBD_{N1}) or in the presence of a 100-fold molar excess of $CaCl_2$ ($CBD_{N1}{\cdot}Ca^{2+}$). DSC thermogram measurements and simulations were executed according to the method of Creagh et al. (*16*). To examine possible buffer effects, experiments were repeated with CBD_{N1} in 50 mM sodium acetate and 50 mM sodium chloride at pH 6.0 using a Model 4215 MC-DSC (Calorimetry Sciences Corp.).

Analysis of Binding Kinetics. Calcium association/dissociation kinetics were determined by line shape analysis of the $^1H^N$ and/or ^{15}N signals from amides showing intermediate two-site chemical exchange during the titration of CBD_{N1} with this metal ion. This analysis was done manually by matching the experimental line shape and frequency of selected resonances with those from simulated spectra based on the formalism described by Sandström (*17*). The experimental 1D ^1H and 2D $^1H-^{15}N$ HSQC spectra were processed using only a 2 Hz line broadening window function. Spectral simulations were obtained using values for the fraction of protein bound (f_b), the total change in chemical shift of a given nucleus between the bound and free forms ($\Delta\delta_{total}$), the dissociation rate constant (k_{off}), and the transverse relaxation times for the ^1H or ^{15}N nucleus in the free (T_{2f}) and bound (T_{2b}) state. Values of f_b were calculated using the previously determined equilibrium binding constant (K_a) for $CaCl_2$ by CBD_{N1}. Values of T_{2f} and T_{2b} were estimated from the full line widths at half-height, and checked by comparison of the experimental and calculated line shapes for free (apo-CBD_{N1}) and fully calcium-saturated protein ($CBD_{N1}{\cdot}Ca^{2+}$), respectively. Spectra were then simulated as a function of k_{off} using a program written by Michael Strain (University of Oregon) that runs

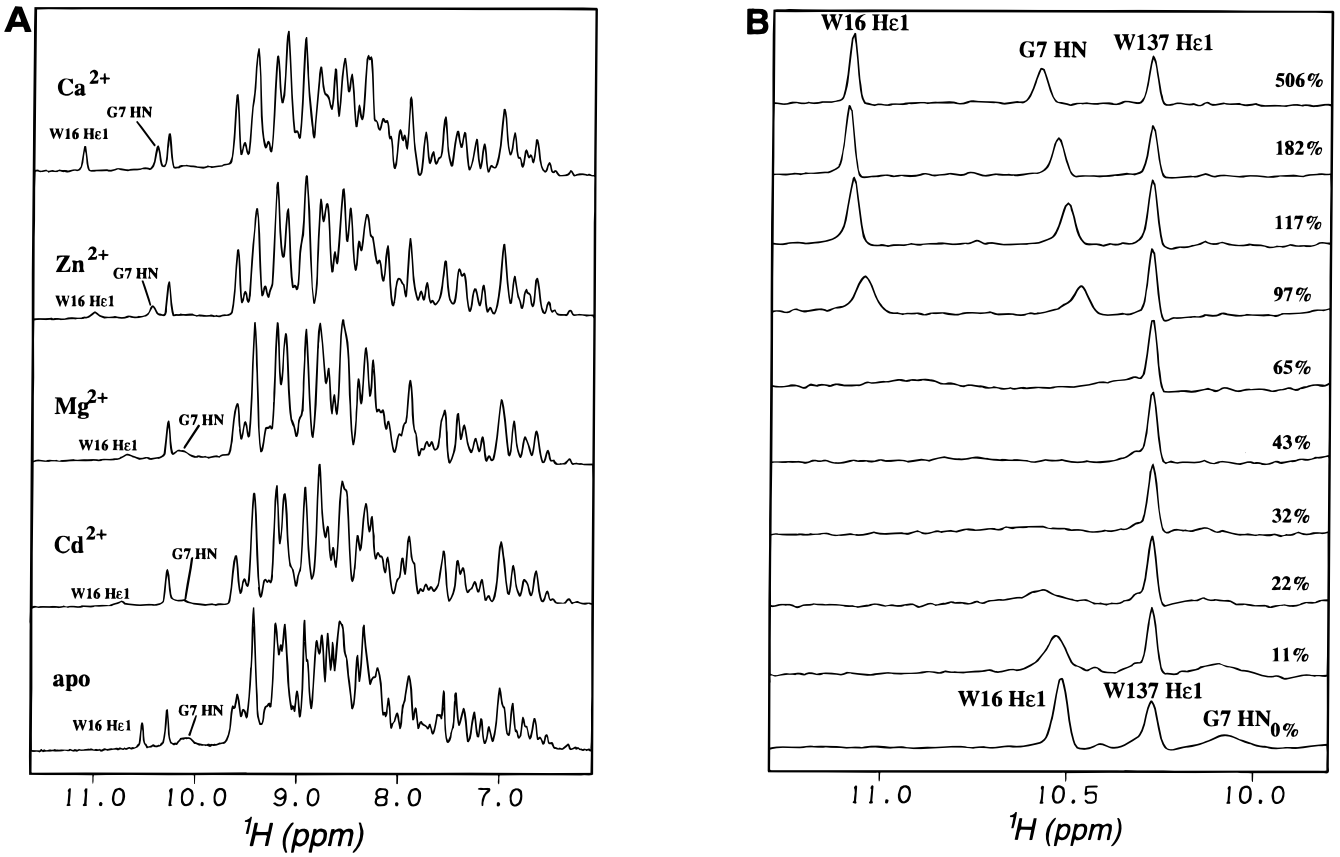

FIGURE 1: (A) CBD_{N1} binds the divalent cations Ca^{2+}, Zn^{2+}, Cd^{2+}, and Mg^{2+} as evident by spectral changes, such as the perturbations of the resonances from Gly7 H^N and Trp16 $H^{\epsilon 1}$, that result from the addition of a 10-fold molar excess of each metal chloride (4.0 mM) to the protein at pH* 6.0 and 35 °C. Since Cd^{2+} and Mg^{2+} bind weakly, these metal ions cause chemical shift changes indicative of partial saturation. The nonuniform excitation profile results from the use of a 1-1 echo pulse sequence. (B) Titration of ^{15}N-labeled CBD_{N1} with $CaCl_2$ as monitored by ^{15}N-decoupled one-dimensional NMR spectroscopy. The percentage molar ratio of calcium-to-protein is indicated. At partial saturation, the resonances from Gly7 H^N and Trp16 $H^{\epsilon 1}$ are line-broadened due to calcium binding on the time scale of intermediate exchange.

as a macro in FELIX v2.3. The association rate constant was then calculated from the relationship $k_{on} = k_{off}K_a$.

RESULTS

CBD_{N1} Binds Divalent Metal Ions. The binding of CBD_{N1} to a series of diamagnetic metal ions (Ca^{2+}, Zn^{2+}, Cd^{2+}, and Mg^{2+}) was screened by one-dimensional NMR spectroscopy. Based upon the numerous perturbations of the spectrum of CBD_{N1} resulting from the addition of each ion, including changes in the chemical shifts and line widths of the downfield peaks from Gly7 H^N and Trp16 $H^{\epsilon 1}$, we conclude that all four metals are bound by this protein (Figure 1A). Qualitatively, Ca^{2+}, Zn^{2+}, Cd^{2+}, and Mg^{2+} produce similar changes in the spectrum of CBD_{N1}, indicating that each binds at the same location in this CenC domain. However, the magnitudes of the spectral changes resulting from the addition of 10-fold molar excess of each metal to the same concentration of protein differ, and thus the apparent affinity of CBD_{N1} for these divalent cations decreases in the order $Ca^{2+} > Zn^{2+} > Cd^{2+} \sim Mg^{2+}$. Comparable spectral perturbations were observed previously upon the addition of cellotetraose to CBD_{N1} (*4*), confirming that the original sample of sugar was indeed contaminated with metal ions.

Calcium Binding: Stoichiometry and Association Constant. After the initial screen for metal binding, the interaction of calcium with CBD_{N1} was studied in detail using one- and two-dimensional NMR spectroscopy (Figures 1B and 2). Assignments of the resonances from the amide $^1H^N$ and ^{15}N nuclei in apo-CBD_{N1} and CBD_{N1}·Ca^{2+} were obtained using a suite of multidimensional heteronuclear correlation experiments, combined with montoring the chemical shifts of these groups as a function of added calcium (*4*, and unpublished data). Based on the chemical shifts of peaks, such as those arising from Trp16 $H^{\epsilon 1}$ and Gly7 H^N, it is estimated that without steps taken to remove metal ions, freshly prepared samples of CBD_{N1} are approximately 20% calcium-loaded. The absence of resonances from 13 amides in the spectrum of untreated CBD_{N1} results from line broadening due to calcium binding on the time scale of intermediate chemical exchange. Addition of EDTA leads to the appearance of all but five of these peaks at chemical shifts corresponding to the metal-free state of the protein (Figures 1 and 2). Based on a detailed ^{15}N relaxation study of CBD_{N1} (in preparation), the resonances from the amides of Gly5, Thr8, Ala68, Val144, and Leu146 most likely remain unidentified in apo-CBD_{N1} due to conformational line broadening.

The changes in normalized $^1H^N$ and ^{15}N chemical shifts of 14 amides in CBD_{N1} versus added calcium are shown in Figure 3. These amides exhibit fast exchange on the NMR chemical shift time scale between the free and calcium-bound forms of this protein, and, as evident from their coincident titration curves, are all affected by the same binding event.

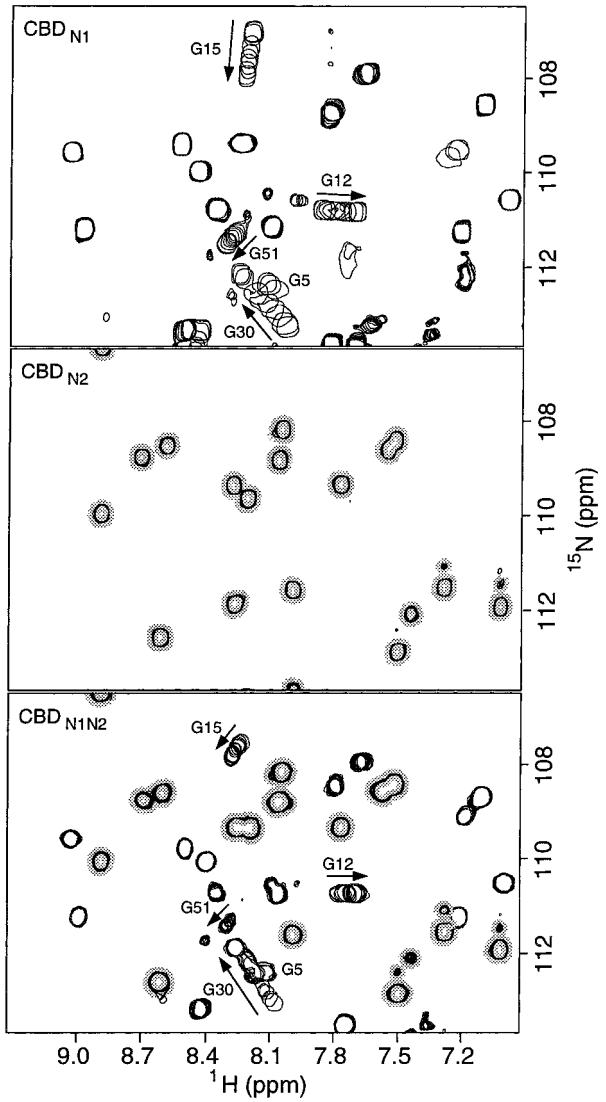

FIGURE 2: Titration of CBD_{N1}, CBD_{N2}, and CBD_{N1N2} with $CaCl_2$ monitored by $^1H-^{15}N$ HSQC spectroscopy. This figure illustrates portions of the overlaid spectra of these three proteins in the presence of increasing amounts of calcium up to a 3−5-fold molar excess. Arrows indicate the directions in which the amide $^1H-^{15}N$ peaks shift upon addition of the metal ion. For the sake of clarity, only selected peaks are assigned. Peaks from the amides of the isolated CBD_{N2} and from the CBD_{N2} portion of the tandem CBD_{N1N2} are identified by shading. Based on the observed chemical shift perturbations, it is evident that CBD_{N1}, both in isolation or as part of the tandem CBD_{N1N2}, binds calcium, whereas CBD_{N2} does not.

Based on the observed plateau in these curves at a metal-to-protein ratio of 1:1, we conclude that CBD_{N1} binds a single calcium ion. The equilibrium constant (K_a) for the association of calcium to this site was determined by a nonlinear least-squares fit of the $^1H-^{15}N$ HSQC chemical shift data to a simple Langmuir isotherm. For each amide, two K_a values were obtained, one using the data for the H^N and the other for the ^{15}N nucleus. In total, 45 fits for 28 different amides (Asp10, Gly12, Gly15, Trp16, Val17, Thr29, Gly30, Ala31, Gly39, Val48, Leu49, Gly51, Val52, Ala53, Arg63, Thr65, Ala66, Ser69, Asp71, Thr73, Leu95, Ser97, Arg100, Val102, Thr105, Leu139, Leu141, and Ala145) were determined, yielding an average K_a of 1.1×10^5 M^{-1} with a standard deviation of 0.5×10^5 M^{-1} at 35 °C and pH* 6.0.

The association of calcium with CBD_{N1} was also investigated using isothermal titration calorimetry (Figure 4).

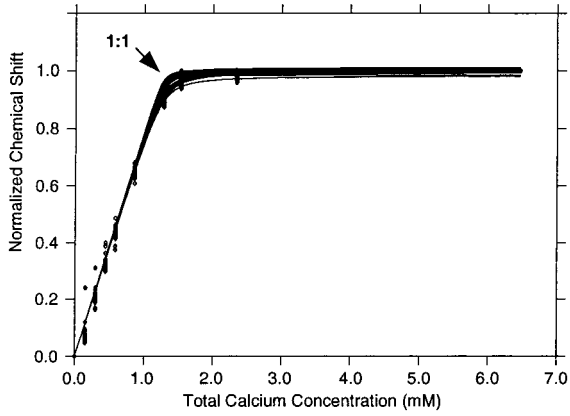

FIGURE 3: CBD_{N1} binds a single calcium ion with an apparent K_a of $(1.1 \pm 0.5) \times 10^5$ M^{-1}. Shown is an overlay of the normalized ^{15}N and $^1H^N$ chemical shifts of 14 amides (Asp10, Gly15, Trp16, Thr29, Gly30, Ala31, Ala53, Arg63, Thr65, Ala66, Ser69, Asp71, Arg100, Leu139, and Leu141) versus the total concentration of added $CaCl_2$. The coincident titration curves indicate that the amides all monitor the same binding event. The arrow marks the plateau where the total calcium concentration equals the total protein concentration (~1.4 mM), demonstrating a stoichiometry of 1:1. The solid lines are the best fits of the data to the Langmuir isotherm describing the binding of a single calcium ion to CBD_{N1}.

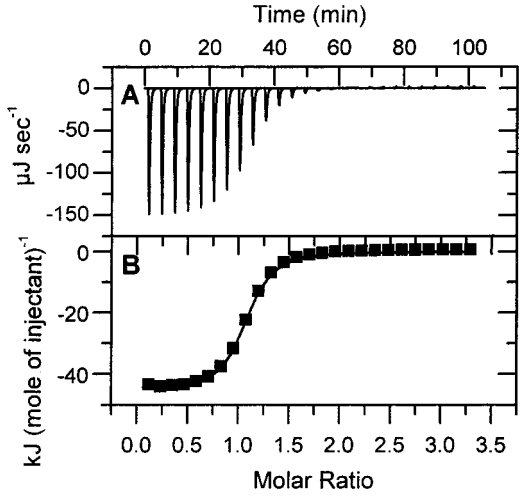

FIGURE 4: Analysis of calcium binding by CBD_{N1} using isothermal titration calorimetry. (A) Raw titration data showing the heat response resulting from each 10 μL injection of 11 mM $CaCl_2$ into the ITC cell containing 0.8 mM CBD_{N1} in 50 mM sodium acetate and 50 mM sodium chloride at pH 6.0 and 35 °C. (B) Peak area normalized to the moles of $CaCl_2$ added and corrected for the heat of dilution (squares), and the nonlinear least-squares fit (line) to a Langmuir isotherm. The average of the best fits for 5 titrations using different titrant and titrand concentrations gives $n = 1.05 \pm 0.04$ calcium ions per CBD_{N1}, $K_a = (1.0 \pm 0.2) \times 10^5$ M^{-1}, and $\Delta H_a = -42 \pm 2$ kJ mol^{-1}.

Analysis of the ITC data demonstrates that the stoichiometry of binding is 1:1 ($n = 1.05 \pm 0.04$) and that the association constant K_a is $(1.0 \pm 0.2) \times 10^5$ M^{-1} at pH 6.0 and 35 °C in 50 mM sodium acetate and 50 mM sodium chloride. Therefore, the results obtained by spectroscopic and calorimetric methods are in excellent agreement. The enthalpy of association (binding) ΔH_a is -42 ± 2 kJ mol^{-1} under these conditions. The binding enthalpy was also measured as a function of temperature from 25 to 40 °C (data not shown). Between 25 and 35 °C, a linear relationship exists, the slope of which gives a heat capacity change upon calcium binding, $\Delta C_{p,a}$, of -0.41 ± 0.16 kJ mol^{-1} K^{-1}. As shown

in the DSC thermogram for apo-CBD_{N1} (Figure 6), the protein is completely folded at temperatures below ~33 °C. However, at 40 °C, a significant fraction of the protein is denatured, and thus the ITC data measured at this temperature are associated with both the refolding of CBD_{N1} and the binding of calcium. As a result, the measured enthalpy of association at 40 °C deviates from the linear temperature dependence defining $\Delta C_{p,a}$.

To determine if displacement of sodium by calcium at the binding site of CBD_{N1} contributes to the binding thermodynamics reported here, the ITC titration was repeated in tetramethylammonium chloride buffer at pH 6.0 and 35 °C. The bulky cation of this salt should not associate to the metal-binding site in CBD_{N1}. Under these conditions, the K_a increases by a factor of only 2. This change lies on the border of statistical significance in an ITC experiment where K_a is on the order of 10^5 M^{-1}. The binding enthalpy ΔH_a also remains unchanged at -42 ± 3 kJ mol^{-1}. Together this indicates that any competing effects of the sodium ion are very small, and implies that the binding site is specific for divalent cations.

Kinetics of Calcium Binding. The kinetics of the association and dissociation of calcium and CBD_{N1} were determined from a line shape analysis of nuclei, such as Trp16$H^{\epsilon 1}$ and Gly7 H^N, that exhibit intermediate exchange on the NMR time scale. As expected from the classical model of two-site chemical exchange, the signals from these nuclei appear as sharp peaks in apo-CBD_{N1} and $CBD_{N1}{\cdot}Ca^{2+}$, yet are severely broadened under conditions of partial saturation. Seven different line shapes from six residues in CBD_{N1} were analyzed according to the formalism of Sandström (*17*). These were the ^1H line shape of Trp16 $H^{\epsilon 1}$ obtained from one-dimensional spectra, and the ^1H line shapes of Gly30, Ala31, Leu139, Leu141, and Ala145 and the ^{15}N line shape of Gly30 obtained from $^1H-^{15}N$ HSQC spectra collected during the titration of this protein with $CaCl_2$. Values for k_{off} were obtained by simulation of the spectrum of each nucleus at as many of the titration points as possible to yield an average k_{off} for each peak (Figure 5). From these individual points, a global average of 4.5×10^2 s^{-1} with a standard deviation of 0.6×10^2 s^{-1} was established for the dissociation rate constant of the $CBD_{N1}{\cdot}Ca^{2+}$ complex. A value for k_{on} of $(5 \pm 2) \times 10^7$ M^{-1} s^{-1} was then calculated from the experimentally determined K_a and k_{off} values.

Effect of Calcium on Cellopentaose Binding by CBD_{N1}. Calcium-saturated CBD_{N1} was titrated with cellopentaose to determine if the presence of the metal ion alters the affinity of the protein for cellooligosaccharides. As was found with a sample of ~20% calcium-loaded CBD_{N1} (*4*, *5*), the stoichiometry of the $CBD_{N1}{\cdot}Ca^{2+}$ complex with cellopentaose is 1:1. This is revealed by the coincident titration curves, measured for each amide by $^1H-^{15}N$ HSQC experiments, with plateaus at a total cellopentaose concentration equal to that of the protein (data not shown). An average K_a for cellopentaose of $(3.1 \pm 0.8) \times 10^4$ M^{-1} was determined by fitting the $^1H^N$ and ^{15}N chemical shifts of 14 different amides (Val17, Tyr19, Gly20, Val34, Gly44, Val45, Leu49, Arg75, Asn81, Gly83, Thr87, Gly130, Gly131, and Leu139) in $CBD_{N1}{\cdot}Ca^{2+}$ to the Langmuir isotherm for a single binding event. This is very similar to the value of $(3.4 \pm 0.8) \times 10^4$ M^{-1} measured previously for ~20% calcium-loaded CBD_{N1} under similar experimental conditions (*4*). Therefore, the affinity of CBD_{N1} for cellopentaose is not dependent upon the binding of calcium.

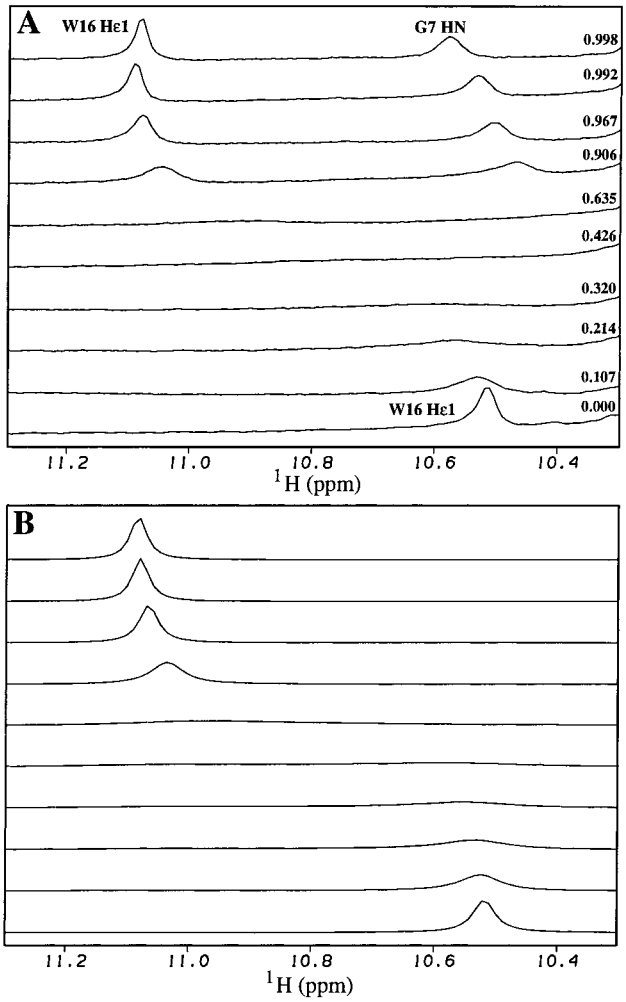

FIGURE 5: Kinetics of calcium binding by CBD_{N1} were determined by line shape analysis according to a two-site exchange model *(17)*. A comparison of the (A) experimental and (B) simulated line shapes of Trp16 $H^{\epsilon 1}$ is shown. The experimental data are an expanded region of the one-dimensional ^1H NMR spectra presented in Figure 1B, with the fraction of total protein in the calcium-bound form indicated for each point in the titration. The simulated line shapes were produced using a k_{off} value of 500 s^{-1}, T_2 values of 0.02 s (free) and 0.015 s (bound), and a difference in frequency of 283 Hz between the free and calcium-bound states of CBD_{N1}.

Effect of Calcium on the Thermodynamic Stability of CBD_{N1}. Thermal denaturation of CBD_{N1} follows a fully reversible two-state transition at all solution conditions examined in this study (*16*). Experimental thermograms are therefore well represented by the van't Hoff equation. Figure 6 shows DSC thermograms for CBD_{N1} at two extreme conditions of calcium loading. In the absence of calcium, reversible unfolding of apo-CBD_{N1} occurs at a midpoint temperature of 46.7 °C with a van't Hoff unfolding enthalpy ΔH_u of 392.0 kJ mol^{-1}. With calcium ion bound at stoichiometric levels, the midpoint unfolding temperature of $CBD_{N1}{\cdot}Ca^{2+}$ rises by approximately 8 °C to 55.2 °C. This represents a significant increase in protein thermal stability, such that at 35 °C, the native state of CBD_{N1} is stabilized by an additional -14 kJ mol^{-1} of Gibbs energy. Consistent with the stabilizing effect of calcium, a midpoint unfolding temperature of 51.2 °C at pH 6.1 was reported previously for CBD_{N1} that, unknown at the time, was partially saturated

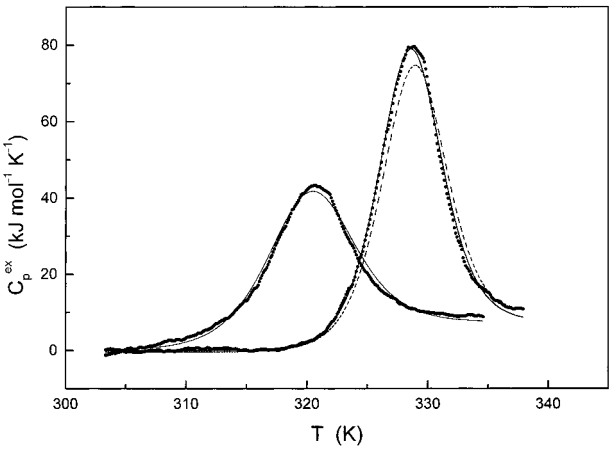

FIGURE 6: DSC thermograms for the unfolding of apo-CBD_{N1} (100-fold molar excess EDTA; $T_m = 46.7$ °C and $\Delta H_u = 392.0$ kJ mol^{-1}) and calcium-saturated CBD_{N1}·Ca^{2+} (100-fold molar excess $CaCl_2$; $T_m = 55.2$ °C and $\Delta H_{total} = 518.2$ kJ mol^{-1}) in 50 mM cacodylate buffer at pH 6.0. The circles are the experimental data, while the solid lines represent the nonlinear least-squares fit to a two-state model of unfolding. The dashed line is the curve predicted for CBD_{N1}·Ca^{2+} using the enthalpy of unfolding measured for calcium-free CBD_{N1}, along with the calcium-binding enthalpy ΔH_a (−42 kJ mol-^{1}) and heat capacity change $\Delta C_{p,a}$ (−0.41 kJ mol^{-1} K^{-1}) obtained from ITC studies.

with calcium (*16*). Note that although calcium has a pronounced effect on the thermal stability of CBD_{N1}, its presence does not significantly change the thermodynamics of sugar binding reported in either Tomme et al. (*5*) or Creagh et al. (*16*). This is because the affinity of CBD_{N1} for cellooligosaccharides, such as cellopentaose, is independent of calcium and is not strongly temperature dependent ($\Delta C_{p,a} = -0.21$ kJ mol^{-1} K^{-1}; *5*).

Calcium-loaded CBD_{N1}·Ca^{2+} is characterized by a total unfolding enthalpy ΔH_{total} of 518.2 kJ mol^{-1} at 55.2 °C and pH 6.0. Identical energetics were measured with both 50 mM cacodylate and 50 mM acetate/50 mM sodium chloride buffers (i.e., those used in the DSC and ITC/NMR experiments, respectively; data not shown). This total unfolding enthalpy is the sum of the heats due to calcium dissociation and CBD_{N1} unfolding, $\Delta H_{total} = -\Delta H_a + \Delta H_u$. Using a measured $\Delta C_{p,u}$ of 7.5 kJ mol^{-1} K^{-1} for the unfolding of CBD_{N1} (*16*), ΔH_u at 55.2 °C is calculated to be 455.8 kJ mol^{-1}. Therefore, calcium dissociation contributes 62.4 kJ mol^{-1} to the ΔH_{total} measured at 55.2 °C for CBD_{N1}·Ca^{2+}. This in turn corresponds to a calculated calcium-binding enthalpy ΔH_a of −58.9 kJ mol^{-1} at 46.7 °C and −54.1 kJ mol^{-1} at 35.0 °C, determined using the observed $\Delta C_{p,a}$ of −0.41 kJ mol^{-1} K^{-1}. This is in reasonable agreement with the exothermic binding enthalpy ΔH_a of -42 ± 2 kJ mol^{-1} measured at 35 °C by ITC. Figure 6 also shows a predicted unfolding thermogram for CBD_{N1}·Ca^{2+} based on the thermodynamics of calcium binding measured by ITC, the DSC thermogram for apo-CBD_{N1}, and the two-dimensional global minimization model of Creagh et al. (*16*). The predicted thermogram and van't Hoff enthalpy are in close agreement with the DSC results measured for CBD_{N1}·Ca^{2+}, indicating a consistent quantitative linkage between calcium binding and protein stability.

Identification of the Calcium-Binding Site in CBD_{N1}. As shown in Figure 2 and summarized in Figure 7, many amides in CBD_{N1} experience a change in their $^1H^N$ and/or ^{15}N chemical shift upon calcium binding. When discussing these changes, it is important to note that chemical shift perturbations can arise either directly from the interaction of the nucleus with the ligand or indirectly from conformational changes resulting from the formation of a protein−ligand complex. Chemical shifts are also a very sensitive indicator of structure, with subtle conformational changes often leading to relatively large changes in shift. Keeping this in mind, it is possible to gain insight into the location of the metal-

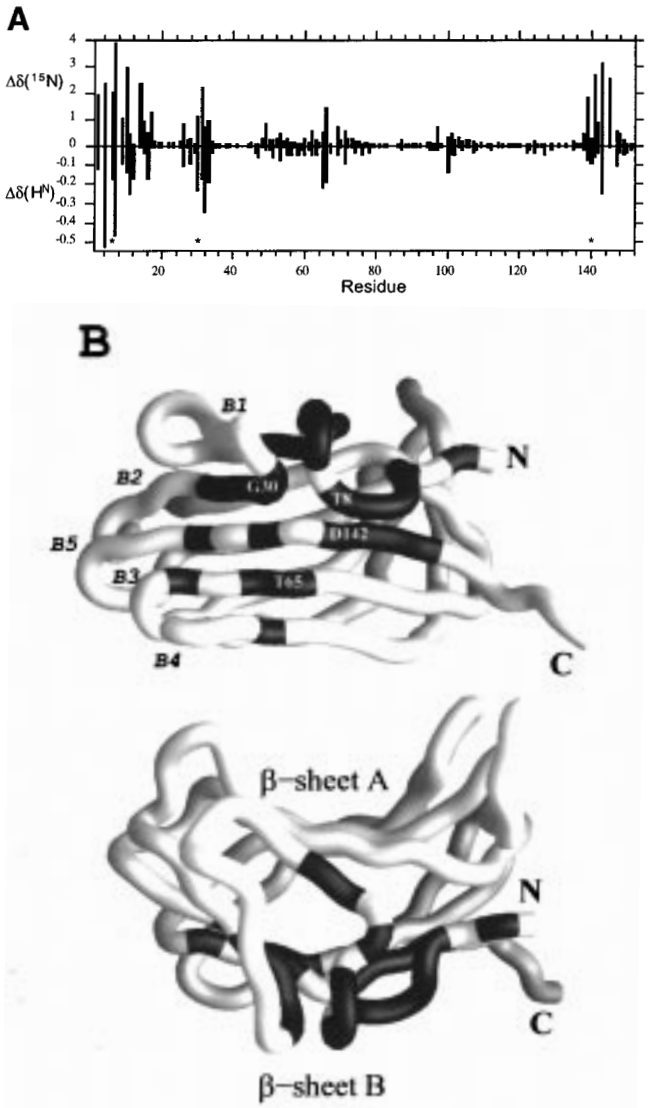

FIGURE 7: (A) Identification of the metal-binding site in CBD_{N1} based on the observed patterns of chemical shift perturbation resulting from calcium binding. The absolute values of the differences between the ^{15}N and $^1H^N$ chemical shifts (ppm) of the backbone amides in the free and calcium-bound forms of the protein are plotted as positive and negative numbers, respectively. The regions showing the greatest change in chemical shift involve the postulated ligating residues Thr8, Gly30, and Asp142, which are marked by asterisks. (B) A C^α worm diagram of CBD_{N1} with the residues that experience the largest changes in chemical shift upon calcium binding, or whose amide resonances are not detected in the absence of added calcium (Gly5, Thr8, Ala68, V144, Leu146), identified in black. The top panel shows β-sheet B, which lies opposite to the oligosaccharide-binding face that is formed by β-sheet A (*6*). The molecule is rotated by 90° in the lower panel to provide a view through the binding cleft. Selected residues are labeled, and the amino and carboxyl termini are denoted by N and C, respectively. This figure was created using the program GRASP (*33*).

binding site in CBD_{N1} from the patterns of amide chemical shift perturbations accompanying the addition of calcium to the protein (Figure 7A). To this end, the residues of CBD_{N1} that experience the largest change in either ^{15}N or H^N chemical shift, as well as those not detected in the absence of added metal (Gly5, Thr8, Ala68, Val144, Leu146), are identified on a worm diagram of CBD_{N1} (Figure 7B).

Based on the data presented in this figure, it is clear that the chemical shifts of amides from five regions of CBD_{N1} are strongly influenced by calcium binding. These include the N-terminus up to residue Val17, Gly30−Cys33 (β-strand B2), Thr65−Ala68 (β-strand B3), Leu139−Leu146 (β-strand B5), and Arg100 (β-strand B4). When mapped onto the tertiary structure of CBD_{N1}, these residues all lie on the face of the protein formed by the N-terminal amino acids and β-sheet B (*6*). In contrast, with the exception of Trp16 and Val17, no amides on the oligosaccharide-binding face (β-sheet A) of the protein show a significant change in chemical shift upon formation of the $CBD_{N1}{\cdot}Ca^{2+}$ complex.

The titration of calcium into CBD_{N1} was also monitored by following chemical shifts of the methyl groups in a sample of 10% ^{13}C-enriched protein (data not shown). The methyl peaks that are affected by calcium binding are those from Thr8$^{\gamma 2}$, Ile4$^{\gamma 2}$, Leu32$^{\delta 1}$, Leu49$^{\delta 2}$, Leu49$^{\delta 1}$, and Ala68$^{\beta}$, in order of decreasing chemical shift change. With the exception of Leu49, each of these residues is located in the N-terminal region of CBD_{N1} or in β-sheet B.

Distilling the patterns of the calcium-dependent amide and methyl chemical shift perturbations shown in Figure 7, we conclude that the metal-binding site of CBD_{N1} lies on the face of the protein formed by its N-terminus and β-sheet B. The changes in the resonances of the amides of Trp16 and Val17, located within the oligosaccharide-binding cleft of β-sheet A, are attributed to their proximity to the N-terminus of CBD_{N1}. The changes in the methyl resonances of Leu49 are explained as an indirect conformational effect of calcium binding due to its packing against the aromatic ring of Trp16.

Calcium Binding by CBD_{N1N2}. In the native enzyme CenC, CBD_{N1} exists in tandem with a second family IV CBD (CBD_{N2}). The titrations of the isolated CBD_{N2} and the combined CBD_{N1N2} with $CaCl_2$ were also studied using $^1H-^{15}N$ HSQC spectroscopy (Figure 2). These data clearly reveal that CBD_{N2} does not bind calcium appreciably as its amide $^1H^N$ and ^{15}N resonances remain completely unperturbed upon addition of a 3-fold molar excess of this metal ion. The spectrum of CBD_{N2} is also unchanged after treatment with EDTA, eliminating the possibility of a tightly bound calcium ion that copurifies with the protein (data not shown). In contrast, the $^1H^N$ and ^{15}N resonances from numerous amides in CBD_{N1N2} shift upon the addition of $CaCl_2$. Therefore, the tandem CBD does bind this metal ion.

The $^1H-^{15}N$ HSQC spectrum of the 296 residue CBD_{N1N2} is almost identical to that obtained simply by superimposing the individual spectra of CBD_{N1} and CBD_{N2}, indicating that the two domains are, to the first approximation, structurally independent. This allows for the nearly complete assignment of amide resonances from CBD_{N1N2} using results obtained for the two isolated binding domains. Based on these assignments, we conclude that the amides in CBD_{N1N2} whose chemical shifts are perturbed upon the binding of calcium are located within the N-terminal CBD_{N1} portion of this molecule. Small differences in the magnitudes of these chemical shift perturbations for corresponding residues in the two proteins may reflect slight differences in experimental conditions or subtle effects of CBD_{N2} on the structure of CBD_{N1}. Furthermore, a stoichiometry of 1:1 and a calcium association constant K_a of $(1.2 \pm 0.4) \times 10^5$ M^{-1} were determined for CBD_{N1N2} based on fitting the observed changes in the ^{15}N and $^1H^N$ chemical shifts of 14 amides to a Langmuir isotherm (data not shown). Within experimental error, this is equal to the K_a determined for CBD_{N1} by both NMR and ITC methods. Therefore, whether in isolation or in context of CBD_{N1N2}, the N-terminal CBD_{N1} binds a single calcium ion with an affinity that is not affected by the presence of its partner CBD_{N2}.

DISCUSSION

Location of the Metal-Binding Site and the Structure of $CBD_{N1}{\cdot}Ca^{2+}$. Chemical shift perturbations provide a qualitative indicator of the location of the calcium-binding site on the face of CBD_{N1} formed by its N-terminus and β-sheet B, but do not unambiguously identify the coordinating atoms. Therefore, the regions of CBD_{N1} showing the greatest spectral change upon addition of calcium (Figure 7) were examined structurally for the presence of possible atoms that commonly interact with metal ions. Following this approach, two potential binding sites were identified. The first is the loop region, formed by residues 6−11, that contains Glu6, Asp10, and Asp11. In the minimized average structure of CBD_{N1}, the side chain of Glu6 points away from Asp10 and Asp11 (*6*). However, this region has the highest rms deviations in the structural ensemble, and thus the exact location, or locations, of these side chains may not be accurately defined. The second potential calcium-binding site includes Asp142 and Asp143 in β-strand B5.

In contrast to CBD_{N1}, CBD_{N2} does not bind calcium. Thus, it is expected that the metal-ligating residues are not conserved between these two proteins. If the amino acid side chains comprising only one of two potential binding sites in CBD_{N1} were conserved, this would provide compelling evidence for the identification of the calcium ligands. However, residues in both possible potential sites exhibit low sequence similarities. Specifically, Glu6, Asp10, and Asp11 in CBD_{N1} correspond to a histidine, a serine, and a glutamate in CBD_{N2}, while Asp142 and Asp143 in CBD_{N1} align with a serine and a glutamine in CBD_{N2}. This does not differentiate the two sites, but it is consistent with the lack of calcium binding by CBD_{N2}.

Strong evidence for the location of the calcium-binding site comes from a comparison of the structure of CBD_{N1} with those of the *Bacillus sp.* 1,3-1,4-β-glucanases. As discussed previously (*6*), these proteins share a common jellyroll β-sandwich fold. In the hybrid *Bacillus* 1,3-1,4-β-glucanase H(A16-M), calcium is bound octahedrally, using Pro9 O, Gly45 O, Asp207 O, Asp207 O$^{\delta}$, and two water molecules as the coordinating ligands (*10*, *18*, *19*). The *Bacillus licheniformis* and *Bacillus macerans* 1,3-1,4-β-glucanase structures use the same ligands to coordinate calcium, but bind with pentagonal−bipyramidal geometry due to the involvement of three water molecules (*11*, *12*). The calcium-binding sites of the 1,3-1,4-β-glucanases are remarkably similar in sequence and structure to the corresponding regions of CBD_{N1}. For example, all have a bulge in the β-sheet

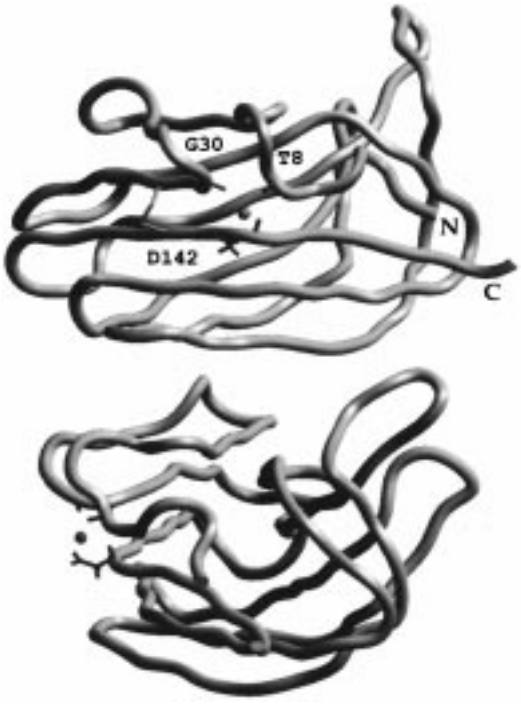

FIGURE 8: Two views of a model of the $CBD_{N1}{\cdot}Ca^{2+}$ complex in which a calcium ion is bound to the postulated ligands Thr8 O, Gly30 O, Asp142 O, and Asp142 O^{δ}. The disulfide bond between Cys33 and Cys140 can also be seen in the upper panel, which presents a direct view of β-sheet B (cf. Figure 7B).

containing Asp207 in the 1,3-1,4-β-glucanases and Asp142 in CBD_{N1}. Also, CBD_{N1} and the hybrid *Bacillus* 1,3-1,4-β-glucanase H(A16-M) have comparable affinity constants for calcium (*18*), and are stabilized thermodynamically by the binding of this metal ion (*18*, *20*−*22*).

In light of these similarities, we postulate that the calcium-binding site of CBD_{N1} is formed by Thr8 O, Gly30 O, Asp142 O, and a side-chain oxygen of Asp142. The adjacent nonconserved Asp143 may also play a role in stabilizing the bound divalent cation through electrostatic interactions. A model of the structure of the $CBD_{N1}{\cdot}Ca^{2+}$ complex, calculated with these four atoms coordinated to a calcium ion, is presented in Figure 8. This model was generated with the identical distance and dihedral angle restraints used to determine the previously reported structure of CBD_{N1} (PDB codes: 1ULO, 1ULP; *6*). It is important to stress that these restraints were in fact measured with samples of CBD_{N1} saturated with cellotetraose and a contaminating metal ion that was most likely calcium. The sugar was not included in the structure calculations due to the lack of NMR assignments for the cellotetraose, while the presence of the bound metal was unsuspected at the time. To generate the model presented in Figure 8, a calcium atom was explicitly included using distance restraints of 2.45 ± 0.15 Å to its postulated main-chain (Thr8 O, Gly30 O, Asp142 O) and side chain (Asp142 O^{δ}) ligating atoms (*23*). While it is possible that the side chain of Asp142 ligates the metal in a bidentate fashion, this is not observed in the 1,3-1,4-β-glucanase structures and thus was not included as a feature of the $CBD_{N1}{\cdot}Ca^{2+}$ model. In almost all calcium-binding proteins, coordination of the metal ion is either octahedral or pentagonal−bipyramidal (*23*). Therefore, it is likely that two or three water molecules also ligate the metal ion bound to CBD_{N1}. We do not have experimental evidence defining the number of water molecules bound to the metal ion in the $CBD_{N1}{\cdot}Ca^{2+}$ complex, and thus the exact geometry of the coordinating ligands shown in Figure 8 could not be determined.

Thermodynamics of Calcium Binding to CBD_{N1}. CBD_{N1} binds calcium with a K_a of ca. 10^5 M^{-1} at pH 6.0 and 35 °C, as determined by both NMR and ITC methods. Similar thermodynamic values (K_a, ΔH_a) were measured in the presence of sodium or tetramethylammonium buffers, indicating that these monovalent cations do not significantly compete with calcium for CBD_{N1}. The same association constant was also measured for CBD_{N1} in the context of the tandem CBD_{N1N2}, demonstrating that its affinity for calcium is not influenced appreciably by the presence of CBD_{N2}. This is consistent with the apparent structural independence of the two neighboring CenC cellulose-binding domains. Finally, the calcium association constant of CBD_{N1} is comparable to that determined for the hybrid *Bacillus* 1,3-1,4-β-glucanase [$(1.0 \pm 0.4) \times 10^5$ M^{-1} at pH 6.0; *18*]. This supports the proposal that the calcium-binding sites of CBD_{N1} and the β-1,3-1,4-glucanase are structurally similar. By way of comparison, K_a values reported for calcium-binding proteins range from $>10^{10}$ M^{-1} for thermitase to $\sim 10^3$ M^{-1} for concanavalin A (*24*), indicating that CBD_{N1} has moderate affinity for this divalent metal ion.

Calcium binding by CBD_{N1} is moderately exothermic with a ΔH_a of −42 kJ mol^{-1} and exhibits enthalpy−entropy compensation ($\Delta S_a = -40.6$ kJ mol^{-1} K^{-1} at 35 °C). Exothermic behavior is often observed in small-ion tight-binding events where coordination between the ion and the ligands is highly favorable. For example, the enthalpy of binding of calcium to EDTA is −29 kJ mol^{-1} at 20 °C and a solution ionic strength of 0.1 M (*25*). It is tempting to argue that the formation of the $CBD_{N1}{\cdot}Ca^{2+}$ complex is driven by enthalpically favorable interatomic interactions which are compensated for entropically by a reduction in the translational and rotational degrees of freedom of the ion and associated protein backbone and side-chain atoms relative to the fully solvated state. However, such an argument is complicated by the role of water. The partial molal desolvation entropy for the calcium ion in water at ambient temperature is 53 J mol^{-1} K^{-1} (*26*), indicating that it is a structure-making solute. Based on the group contribution method of Makhatadze and Privalov (*27*), the dehydration entropies at 25 °C estimated for the postulated calcium ligands in CBD_{N1} are 35 J mol^{-1} K^{-1} (Thr8 O, Gly30 O, and Asp142 O) and 27 J mol^{-1} K^{-1} (Asp142 O^{δ}). Thus, although this analysis is crude, dehydration effects associated with calcium binding appear to be entropically favorable for both the metal ion and the protein ligands. The fact that overall the affinity of calcium for CBD_{N1} is reduced by a net negative entropy change suggests the losses in calcium and protein degrees of freedom dominate desolvation effects. This in turn indicates that the protein adopts a more rigid structure upon binding calcium. Using ^{15}N relaxation measurements, we have observed that residues at the N-terminus of apo-CBD_{N1} and, to a lesser extent, near position 142 exhibit conformational mobility on a micro- to millisecond time scale that is eliminated in the presence of added calcium ions (in preparation).

It is noteworthy that calcium binding to proteins is not often associated with a net loss of entropy (*24*, *28*, *29*). A

striking example is seen with equine lysozyme, where binding is entropically driven and compensated by an unfavorable positive binding enthalpy (*30*). Thus, the relative importance of factors, such as the organization of the solvation layer and the role of conformational dynamics, in establishing the overall affinity for calcium can can differ significantly between proteins.

Kinetics of Calcium Binding to CBD_{N1}. The association rate constant for calcium binding of $(5 \pm 2) \times 10^7$ M^{-1} s^{-1} is within 2 orders of magnitude of the diffusion-controlled limit of $\sim 10^9$ M^{-1} s^{-1}. Similar k_{on} values have been reported for several regulatory EF-hand proteins (*24*). This implies that the calcium-binding site of CBD_{N1} is accessible and, to the first approximation, preformed. That is, no major structural rearrangements or conformational transistions are necessary in the native protein to properly orient the atoms that ligate calcium. This conclusion is consistent with three additional lines of evidence. First, in the structural model of CBD_{N1}·Ca^{2+} presented in Figure 8, the ligating atoms are exposed on the surface of CBD_{N1}. Also, note that Gly30 is located in the loop between β-strands B1 and B2, and Asp142 is within β-strand B5. Thus, two of the three postulated calcium ligands contribute to the jellyroll β-sandwich fold of CBD_{N1}. Second, the residues forming the nascent calcium binding site in apo-CBD_{N1} have $^1H^N$ and ^{15}N chemical shifts indicative of a structured conformation and not a random coil or disordered state (Figure 2; *31*). Furthermore, chemical shift perturbations accompanying the formation of the CBD_{N1}·Ca^{2+} complex are localized to this binding site, rather than being global to the entire protein (Figure 7). Third, we have studied the effects of calcium and oligosaccharide binding on the dynamic properties of CBD_{N1} using ^2H and ^{15}N relaxation methods (in preparation). In summary, we have observed that amides contributing to the metal-binding site are generally well-ordered on the picosecond−nanosecond time scale, in both the free- and calcium-loaded forms of CBD_{N1}. However, this region of apo-CBD_{N1} exhibits conformational exchange between most probably nativelike structures on the micro- to millisecond time scale that become restricted upon calcium binding. This mobility leads to the line broadening seen for Gly7 H^N in Figure 1, and likely precludes the detection of resonances from the amides of Gly5, Thr8, Ala68, Val144, and Leu146 in the metal-free protein. We postulate that conformational plasticity of an approximately preformed binding site allows for the facile association of calcium with CBD_{N1}.

A Structural Role for Calcium Binding by CBD_{N1}. The apparent biological role of calcium binding by CBD_{N1} is to stabilize the folded structure of this protein domain. As determined by DSC, the midpoint denaturation temperature of CBD_{N1} increases by 8 °C in the presence of $CaCl_2$ at pH 6.0. It is tempting to ask whether calcium stabilizes the native structure of CBD_{N1} by binding to three amino acids (Thr8, Gly30, and Asp142) that are distant along the length of its polypeptide chain. However, there does not appear to be a general correlation between the affinity of a protein for calcium, which is thermodynamically linked to its stability, and the number of residues between the chelating atoms (*23*, *24*). This is expected if the metal ion binds only to the folded state of the protein and does not induce a disorder−order transition. Nevertheless, it is intriguing to note that the postulate calcium-binding site in CBD_{N1} is adjacent to the disulfide bond between Cys33 and Cys140. This single disulfide is critical for the integrity of the native CBD_{N1} as its reduction leads to the complete unfolding of the protein (*16*). Studies of the combined effects of metal binding and cysteine oxidation on the stability of CBD_{N1} may prove worthwhile to define the possible linkage between these two factors. It is also of note that CBD_{N2}, which does not bind calcium, has a higher midpoint denaturation temperature than either apo-CBD_{N1} or CBD_{N1}·Ca^{2+} (unpublished observation).

The role of calcium in stabilizing the structure of CBD_{N1} is consistent with the finding that the presence of this cation does not perturb significantly the K_a of the protein for cellopentaose. This is not surprising in light of the fact that the calcium-binding site is on the opposite side of the protein (β-strand B) as is the sugar-binding cleft (β-strand A; Figures 7 and 8). Any structural changes that result upon metal complexation are unlikely to affect residues within the binding cleft. A similar biological role for calcium binding is exhibited by the *Bacillus* 1,3-1,4-β-glucanases. This ion was found to increase the stability of seven native and hybrid 1,3-1,4-β-glucanases against thermal or chemical denaturation (*18*, *21*−*23*). X-ray crystallographic studies reveal that calcium binds at a position distant from the active site cleft of each glucanase, and thus is unlikely to influence their catalytic activities. In contrast, proteins, such as lectins, that exhibit calcium-dependent affinity for sugar often utilize the metal ion directly to aid in carbohydrate binding (*32*).

In general, little is known about the role of metal ion binding by CBDs. A calcium ion has been identified in the crystal structure of CBD_{Cip} (*9*), as well as that of CBD_{E4} (*13*). As in the case of CBD_{N1}, the metal ions are bound at sites distant from the putative cellulose-binding faces of each of these proteins. It is likely that calcium also serves to stabilize the structures of CBD_{Cip} and CBD_{E4}, without directly influencing their affinity for cellulose. Based on these three examples, it is reasonable to suggest that metal binding is one possible mechanism to enhance the stability of cellulases in order to ensure that they remain folded when secreted into potentially harsh natural environments by cellulolytic microorganisms.

ACKNOWLEDGMENT

We thank Dr. David Remeta, Biocalorimetry Center, Johns Hopkins University, for performing the NanoDSC measurements, Dr. Michael Strain, University of Oregon, for providing chemical exchange analysis programs, and Dr. Carolyn Slupsky, Mr. Lloyd MacKenzie, and Ms. Arluk Setter, The University of British Columbia, for helpful advice.

REFERENCES

1. Tomme, P., Warren, R. A. J., and Gilkes, N. R. (1995) *Adv. Microb. Physiol. 37*, 1−81.
2. Tomme, P., Warren, R. A. J., Miller, R. C., Jr., Kilburn, D. G., and Gilkes, N. R. (1995) in *Cellulose-Binding Domains: Classification and Properties* (Saddler, J. N., and Penner, M., Eds.) pp 142−161, American Chemical Society, Washington, DC.
3. Coutinho, J. B., Gilkes, N. R., Warren, R. A. J., Kilburn, D. G., and Miller, R. C., Jr. (1992) *Mol. Microbiol. 6*, 1243−1252.
4. Johnson, P. E., Tomme, P., Joshi, M. D., and McIntosh, L. P. (1996) *Biochemistry 35*, 13895−13906.

5. Tomme, P., Creagh, A. L., Kilburn, D. G., and Haynes, C. A. (1996) *Biochemistry 35*, 13885−13894.
6. Johnson, P. E., Joshi, M. D., Tomme, P., Kilburn, D. G., and McIntosh, L. P. (1996) *Biochemistry 35*, 14381−14394.
7. Kraulis, P. J., Clore, G. M., Nilges, M., Jones, T. A., Pettersson, G., Knowles, J., and Gronenborn, A. M. (1989) *Biochemistry 28*, 7241−7257.
8. Xu, G.-Y., Ong, E., Gilkes, N. R., Kilburn, D. G., Muhandiram, D. R., Harris-Brandts, M., Carver, J. P., Kay, L. E., and Harvey, T. S. (1995) *Biochemistry 34*, 6993−7009.
9. Tormo, J., Lamed, R., Chirino, A. J., Morag, E., Bayer, E. A., Shoham, Y., and Steitz, T. A. (1996) *EMBO J. 15*, 5739−5751.
10. Keitel, T., Simon, O., Borriss, R., and Heinemann, U. (1993) *Proc. Natl. Acad. Sci. U.S.A. 90*, 5287−5291.
11. Hahn, M., Olsen, O., Politz, O., Borriss, R., and Heinemann, U. (1995) *J. Biol. Chem. 270*, 3081−3088.
12. Hahn, M., Planas, A., Querol, E., and Heinemann, U. (1995) *FEBS Lett. 374*, 221−224.
13. Sakon, J., Irwin, D., Wilson, D. B., and Karplus, P. A. (1997) *Nat. Struct. Biol. 4*, 810−818.
14. Delaglio, F., Grzesiek, S., Vuister, G. W., Zhu, G., Pfeifer, J., and Bax, A. (1995) *J. Biomol. NMR 6*, 277−293.
15. Zhang, O., Kay, L. E., Olivier, J. P., and Foreman-Kay, J. D. (1994) *J. Biomol. NMR 4*, 845−858.
16. Creagh, A. L., Koska, J., Johnson, P. E., Tomme, P., Joshi, M. D., McIntosh, L. P., Kilburn, D. G., and Haynes, C. A. (1998) *Biochemistry 37*, 3529−3537.
17. Sandström, J. (1982) *Dynamic NMR Spectroscopy*, Academic Press, London.
18. Keitel, T., Meldgaard, M., and Heinemann, U. (1994) *Eur. J. Biochem. 222*, 203−214.
19. Hahn, K., Keitel, T., and Heinemann, U. (1995) *Eur. J. Biochem. 232*, 849−858.
20. Welfle, K., Misselwitz, R., Wefle, H., Simon, O., Politz, O., and Borriss, R. (1994) *J. Biomol. Struct. Dyn. 11*, 1417−1424.
21. Welfle, K., Misselwitz, R., Wefle, H., Politz, O., and Borriss, R. (1995) *Eur. J. Biochem. 229*, 726−735.
22. Welfle, K., Misselwitz, R., Politz, O., Borriss, R., and Welfle, H. (1996) *Protein Sci. 5*, 2255−2265.
23. McPhalen, C. A., Strynadka, N. C. J., and James, M. N. G. (1991) *Adv. Protein Chem. 42*, 77−144.
24. Linse, S., and Forsén, S. (1995) *Adv. Second Messenger Phosphoprotein Res. 30*, 89−152.
25. Smith, R. M., and Martell, A. E. (1989) *Critical Stability Constants*, Plenum Press, New York.
26. Burgess, J. (1988) *Ions in Solution*, Ellis Horwood Ltd., Chichester, U.K.
27. Makhatadze, G. I., and Privalov, P. L. (1993) *J. Mol. Biol. 232*, 639−659.
28. Vanderheeren, G., Hanssens, I., Meijberg, W., and Van Aerschot, A. (1996) *Biochemistry 35*, 16753−16759.
29. Henzel, M. T., Hapak, R. C., and Goodpasture, E. A. (1996) *Biochemistry 35*, 5856−5869.
30. Griko, Y. V., Freire, E., Privalov, G., Van Dael, H., and Privalov, P. L. (1995) *J. Mol. Biol. 252*, 447−459.
31. Wishart, D., and Sykes, B. (1994) *J. Biomol. NMR 4*, 171−180.
32. Rini, J. M. (1995) *Annu. Rev. Biophys. Biomol. Struct. 24*, 551−577.
33. Nicholls, A., Sharp, K. A., and Honig, B. (1991) *Proteins: Struct., Funct., Genet. 11*, 281−292.

BI980978X